

pubs.acs.org/JCTC Article

Exploring Energy Landscapes of Intrinsically Disordered Proteins: Insights into Functional Mechanisms

Antonio B. Oliveira Junior, Xingcheng Lin, Prakash Kulkarni, José N. Onuchic, Susmita Roy,* and Vitor B. P. Leite*



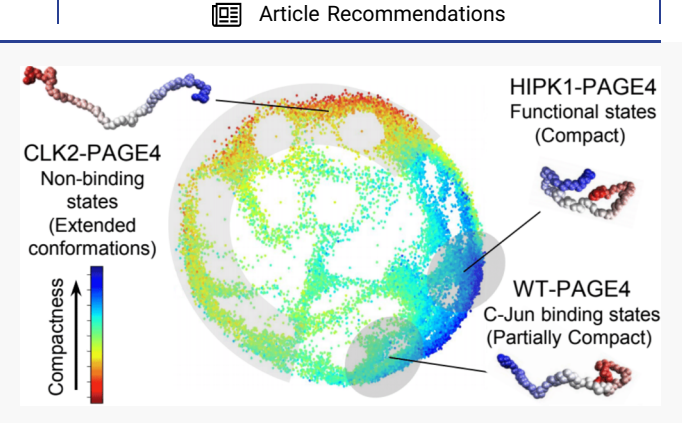
Cite This: J. Chem. Theory Comput. 2021, 17, 3178-3187



ACCESS

III Metrics & More

ABSTRACT: Intrinsically disordered proteins (IDPs) lack a rigid three-dimensional structure and populate a polymorphic ensemble of conformations. Because of the lack of a reference conformation, their energy landscape representation in terms of reaction coordinates presents a daunting challenge. Here, our newly developed energy landscape visualization method (ELViM), a reaction coordinate-free approach, shows its prime application to explore frustrated energy landscapes of an intrinsically disordered protein, prostate-associated gene 4 (PAGE4). PAGE4 is a transcriptional coactivator that potentiates the oncogene c-Jun. Two kinases, namely, HIPK1 and CLK2, phosphorylate PAGE4, generating variants phosphorylated at different serine/threonine residues (HIPK1-PAGE4 and CLK2-PAGE4, respectively) with



opposing functions. While HIPK1-PAGE4 predominantly phosphorylates Thr51 and potentiates c-Jun, CLK2-PAGE4 hyperphosphorylates PAGE4 and attenuates transactivation. To understand the underlying mechanisms of conformational diversity among different phosphoforms, we have analyzed their atomistic trajectories simulated using AWSEM forcefield, and the energy landscapes were elucidated using ELViM. This method allows us to identify and compare the population distributions of different conformational ensembles of PAGE4 phosphoforms using the same effective phase space. The results reveal a predominant conformational ensemble with an extended C-terminal segment of WT PAGE4, which exposes a functional residue Thr51, implying its potential of undertaking a fly-casting mechanism while binding to its cognate partner. In contrast, for HIPK1-PAGE4, a compact conformational ensemble enhances its population sequestering phosphorylated-Thr51. This clearly explains the experimentally observed weaker affinity of HIPK1-PAGE4 for c-Jun. ELViM appears as a powerful tool, especially to analyze the highly frustrated energy landscape representation of IDPs where appropriate reaction coordinates are hard to apprehend.

■ INTRODUCTION

Contrary to Anfinsen's hypothesis that structure defines protein function, ¹ it is now increasingly evident that a significant fraction of the human proteome is composed of intrinsically disordered proteins (IDPs) that lack rigid three-dimensional (3D) structure. ^{2–5} Despite the lack of well-defined structure under physiological conditions at least *in vitro*, IDPs are involved in a large number of biological functions ranging from gene regulation, molecular recognition, signal transduction, and intracellular information processing events, ^{6–8} underscoring their functional significance.

IDPs can adopt a huge repertoire of conformations because of their high backbone flexibility and inherent plasticity ^{9–13} and hence exist as conformational ensembles. Thus, the conformational search process of an IDP involves a higher-dimensional phase space than a structured/ordered protein. While enormous research efforts have been spurred to understand the classical "minimally frustrated" or "funnel-

like" energy landscapes for structured proteins, ^{14–16} understanding "highly frustrated" or "weakly funneled" nature of IDPs has remained far more challenging due to their large-scale conformational changes. ^{17–20} Furthermore, compared to ordered proteins, IDPs are relatively more susceptible to post-transitional modifications, especially phosphorylation, ^{21–23} which has been shown to impinge on their conformational dynamics. ^{7,24–26} In several cases, such conformational switches induced by site-specific phosphorylation have been implicated in disease pathology.

Received: January 8, 2021 Published: April 19, 2021





Concomitant with advances in experimental techniques typically used to investigate IDPs, such as nuclear magnetic resonance (NMR), small-angle X-ray scattering (SAXS), and single-molecule fluorescence resonance energy transfer (smFRET), 27-31 over the past two decades, a number of computational techniques have been developed, causing an explosion in research on the IDPs. 32,33 Nonetheless, capturing the detailed conformational dynamics of IDPs at an atomistic length scale remains a challenge both experimentally and computationally. More specifically, the challenges are two-fold: (i) Generating high-resolution ensemble of highly flexible IDPs is computationally expensive in most cases as a large number of conformational changes are associated with an IDP; (ii) due to the numerous degrees of freedom in complex IDPs, mechanistic interpretation of trajectories from computer simulations is a tough call, if not impossible. The former challenge imparts the sampling issues concerning the huge phase space of IDPs. Canonical atomistic molecular dynamics (MD) simulations are often found futile in simulating IDPs due to inadequate statistical sampling. Ideally, sampling an IDP requires long-time simulations, and these are computationally highly expensive. To address the sampling issues, different coarse-grained (CG) models, ^{34,35} trained molecular simulations by experimental inputs, ^{36–38} de-novo enhanced MD simulations techniques are developed and found quite useful in rapid sampling of the IDP phase space.³⁹⁻⁴¹ While most of the computational techniques focus on the sampling issues of IDPs, which of course is essential, mechanistic interpretation of trajectories from computer simulations still remains a major challenge.

Among IDPs that have been extensively studied, prostateassociated gene 4 (PAGE4) is one of the most wellcharacterized IDPs in terms of its biology and its conformational preferences and dynamics. 25,42,43 PAGE4 is a stressresponse protein that acts as a transcriptional coactivator. In prostate cancer cells, PAGE4 potentiates transactivation of c-Jun that heterodimerizes with c-Fos to form the activator protein-1 (AP-1) complex. 44 The stress-response kinase, homeodomain-interacting protein kinase 1 (HIPK1), phosphorylates PAGE4 predominantly at Thr51 with a minor fraction of the ensemble being phosphorylated at Ser9.⁴⁵ On the other hand, CDC-like kinase 2 (CLK2) hyperphosphorylates PAGE4 (CLK2-PAGE4), and in contrast to HIPK1-PAGE4, CLK2-PAGE4 inhibits c-Jun activity. 43 Consistent with the biochemical data, NMR studies indicated that HIPK1-PAGE4 exhibits stronger binding to AP-1 than CLK2-PAGE4. Furthermore, MD simulations using atomistic associative memory, water mediated structure and energy model (AAWSEM) revealed that this difference in binding affinity may be attributed to the phosphorylation-induced conformational changes adopted by HIPK1-PAGE4 and CLK2-PAGE4. Confirming the results from molecular simulation, SAXS and smFRET results show that HIPK1-PAGE4 exhibits a relatively compact conformational ensemble, whereas the conformational ensemble of CLK2-PAGE4 appears more expanded.⁴³

Given the complexity and 3D spread of the conformational space of an IDP as highly disordered as PAGE4, ^{27,46} deriving an ensemble average picture representing its conformational plasticity may represent a rather crude approach. By this approach, a functional conformational ensemble might stay underestimated. Therefore, visualization of the entire conformational ensemble map is important that can help identify the mechanistic interplay between different conformational

clusters and their functional implications. With this goal in mind, here, we have adopted the energy landscape visualization method (ELViM), a unique and useful tool to discern the rough energy landscapes of IDPs and rich characteristics of IDP dynamics.⁴⁷ Given the data set of conformations and using an appropriate metric, ELViM calculates a matrix of internal distances between all pairs of conformations. This matrix, which represents the data set in the high-dimensional phase space, is then projected into an effective two-dimensional (2D) phase space. The analysis of this final energy landscape representation allows us to infer and establish a connection with functional mechanisms.

METHODS

Brief Description of the AAWSEM Model. The equilibrium simulation trajectories for all PAGE4 phosphoforms were obtained using the AAWSEM force field. AAWSEM is a multiscale model combining explicit-solvent atomistic simulations of local segments of proteins with CG simulations of full protein structures. The model has been shown to successfully fold proteins composed mainly of α helices and of α/β structures, Details of the implementations of AAWSEM models can be found in refs 48 and 50. Briefly, the original AWSEM potential includes a memory term, $W_{\rm FM}$, which guides the local-in-sequence interactions of proteins by using structure templates. In AAWSEM, $V_{\rm FM}$ uses the clustered structures from exhaustive atomistic explicit-solvent simulations as structural templates.

Atomistic Simulations of Different Phosphoforms of PAGE4 and Their Segments. The simulation trajectories of PAGE4 were adopted from an earlier publication. 42 In the simulation of PAGE4, a total of three phosphorylated forms of PAGE4 were studied. WT-PAGE4 used the wild-type PAGE4 sequence. HIPK1-PAGE4 had two sites, Ser9 (30-40%) and Thr51 (>95%), being phosphorylated, where the percentage in parentheses reflects the phosphorylation probability of corresponding residues determined by experiments.²⁷ CLK2-PAGE4 is a hyperphosphorylated form with eight sites being phosphorylated: Ser7 (>95%), Ser9 (>95%), Thr51 (>95%), Thr71 (50%), Ser73 (75%), Ser79 (50%), Thr85 (>95%), and Thr94 (60%). 25 These three forms of PAGE4 were segmented according to the empirical motifs annotated in the literature.²⁷ The segments were solvated and simulated using the CHARMM36m force field,⁵² which gives a balanced treatment of ordered and disordered proteins. The phosphorylated residues were simulated by adding phosphoryl groups onto the original residues in the atomistic simulations. To enhance sampling of different conformations of proteins, the continuous simulated tempering (CST) method⁵³ was employed in the atomistic simulations, with temperature varying from 293 to 350 K. To best represent the structures sampled at physiological temperature, from these atomistic simulations, we only feed those structures sampled with temperatures between 293 and 330 K to process through CG AAWSEM forcefield. The atomistic simulations were carried out with the GROMACS software package. 54,55 Each segment was simulated for at least 1 μ s, and the first 25 ns of each trajectory was removed as required for convergence of the CST algorithm.

AAWSEM Simulations of Different Phosphoforms of PAGE4. The clustered fragment structures from the atomistic simulations of different phosphorylated forms of PAGE4 were separately included as template structures for $V_{\rm FM}$ in the

AAWSEM simulations of the corresponding full protein. The AAWSEM simulations of three phosphorylated forms of PAGE4 were carried out with a constant temperature of 300 K maintained by the Langevin thermostat. 36 Electrostatic interactions were treated using the Debye-Hückel approximation,⁵⁷ with a Debye screening length of 10.0 Å. Electrostatic interactions were also scaled by 4.0 to achieve a relatively balanced strength compared to the other terms of the AAWSEM potential. Since the original AWSEM potential leads to an overly compact ensemble in simulations of disordered proteins, the nonbonded contact potential of AWSEM was modified to better reflect the size distribution of disordered proteins. Details about the choice of parameters as well as the simulated trajectories of PAGE4 were discussed in our previous paper. 42 The phosphorylated residues of PAGE4 were modeled by replacing the phosphorylated residues with "supercharged" (-2e) glutamic acid (Glu) residues. 58,59 Furthermore, to reflect the phosphorylation probabilities of these residues, we multiplied their charges by the phosphorylation probabilities. Our simulation quantitatively reproduced the size distribution of three phosphorylated forms of PAGE4, as measured by SAXS and smFRET experiments, 25 as well as the change of local secondary structures upon phosphorylation, indicated by the NMR experiments.2

ELViM. The visualization of biological macromolecule landscapes is achieved by optimizing a 2D representation of distances between structures of a given data set of conformations. The method is based primarily on computing a matrix with effective distances between all pairs of structures. For two conformations k and l, their similarity measurement is given by

$$q^{k,l} = \frac{1}{N} \sum_{N} \exp \frac{-(r_{i,j}^{k} - r_{i,j}^{l})^{2}}{\sigma_{i,j}^{2}}$$
(1)

where $r_{i,j}k(1)$ is the distance between the atoms i and j of the conformation k(l). N is the normalization over all non-neighboring pairs of residues and $\sigma_{i,j} = \sigma_0 |i-j|^c$, with $\sigma_0 = 1 \text{ Å}^2$ and $\epsilon = 0.15$. The dissimilarity between any two structures is described as

$$\delta^{k,l} = 1 - q^{k,l} \tag{2}$$

where $\delta^{k,l}$ ranges from 0 (identical) to 1 (very different). The method seeks to represent every state of the data set by a point in a 2D phase space, which aims to describe the computed effective distances in an optimal manner. The method goes beyond the usual one-dimensional representation, and it does not require a reference conformation or a reaction coordinate. This approach relies only on structural information, but the states' energies are implicitly accounted for since they are strongly correlated with their molecular conformations.

The visualization method is based on four steps: (i) An ensemble of structures which, in general, are obtained through simulations is generated; (ii) the dissimilarity matrix is calculated by applying a metric throughout the simulated trajectory; (iii) a data processing procedure may be carried out to cluster very similar structures into a single conformation, lowering the effective total number of conformations to be analyzed; (iv) a multidimensional projection is performed and, then, the dissimilarity matrix is transformed to a 2D projection.

There are many methods for the analysis of complex multidimensional data which rely on pairwise distances between elements. 62 The most common are those used for

hierarchical phylogenetic trees, including extremely diverse systems, such as the phylogenetic tree of life. 63 In comparison, a conformational phase space of a given protein is much simpler, and a phylogenetic tree is a valuable approach for clustering analysis, 64,65 which has used the exact pairwise distance definition as in eq 2.66 However, such studies are limited to local clustering. In the ELViM, all protein conformations are projected into a 2D phase space without a clustering procedure. If the studied system is too complex, such a bold trial is not always expected to provide meaningful results. However, if the system is not too complex, which is what we have observed so far, it is expected this simplified representation to reveal a rich picture of the underlying landscape. ELViM can automatically detect pathways and competing transition-state ensembles without the need for an a priori reaction coordinate. Instead of having to intuitively design coordinates, which can involve visual inspection of large numbers of transition events, ELViM provides a means for efficiently mapping structurally distinct pathways, which are observed in conformational rearrangement in multidomain, or multicomponent, and assemblies.

From ELViM projection, the density of states (DOS) of each region or pixel can be obtained (n_i) , from which the 2D free energy can be inferred as

$$\mathcal{F} = -k_{\rm B}T \, \log(n_i/N) \tag{3}$$

where N is the total number of conformations. The local minima can be associated with the more stable conformation basins and saddle points to transition states between basins of stability, which allow us to estimate energy barriers, as we see in the present study.

In this work, we propose a slightly different analysis; we carry out the projection for different systems simultaneously using the same phase space. In this case, 10,000 structures of each simulation separately were selected (WT, CLK2, and HIPK1); from these data, we performed the steps (ii) and (iv) described above in order to obtain the effective 2D projection as results. The information about which simulation each structure belongs to is preserved and can be labeled.

■ RESULTS

The simulation trajectories of PAGE4 consist of 10⁴ configurations of each of the three variants: wildtype (WT), CLK2, and HIPK1, which were described in a previous study. 42 The sequence of PAGE4 and its phosphorylated and nonphosphorylated (WT) residues are indicated in Figure 1a. In this work, we have employed our newly developed ELViM for the first time to not only visualize and understand the higher-dimensional conformational phase space of a highly flexible IDP but also compare the different conformational ensembles. ELViM being a reaction coordinate-free method nicely provides an unprecedented and intuitive 2D visualization of the multidimensional phase space. The effective 2D phase space of all PAGE4 conformers is given by an approximately circular disk, shown in Figure 1b, in which, each structure is represented by a point. One can see the conformational states of WT-PAGE4 and HIPK1-PAGE4 occupying similar regions of the phase space, while CLK2-PAGE4 occupies a region in the phase space that is distinct from that occupied by the WT and HIPK1 ensembles. However, ELViM brings all conformational ensembles of each conformer under the same effective phase space region

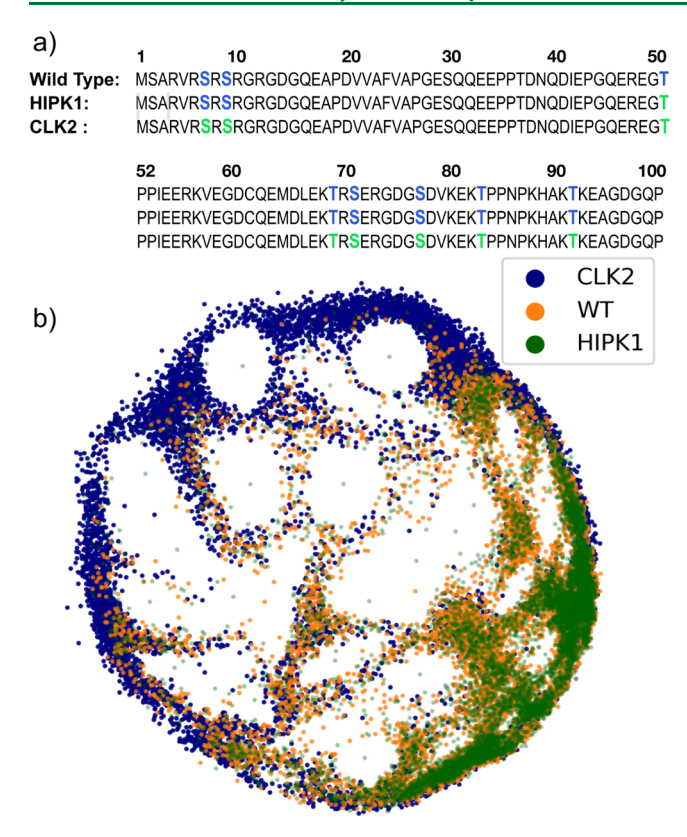


Figure 1. PAGE4 sequences and 2D ELViM projection. (a) PAGE4 wild type, HIPK1, and CLK2 sequences, in which the non-phosphorylated and phosphorylated residues are shown in blue and green, respectively. (b) Each configuration of each type of phosphoform is represented as a point in the ELViM's effective 2D representation.

where the ensemble overlaps and distinctions can be discerned simultaneously.

Validation of 2D Phase Space. If the studied system is not very complex, ELViM can provide a meaningful energy landscape of the structures. One way to validate ELViM representation is to probe measurable variables and determine if they are well behaved, that is, if they vary continuously. Figure 2 shows the radius of gyration (R_{σ}) of different regions of the protein for each state where different conformations are enveloped. This analysis is consistent with our early simulation measurements and indeed captures the dynamical changes in the PAGE4 ensemble. By separately accounting for N- and Cterminal regions, we previously observed that both N- and Cterminal regions have a loop-forming tendency. 43 However, the present study revealed that the N-terminal part more frequently adopts a compact turnlike structure compared to the C-terminal region (Figure 2b,c). This clearly implies that the N-terminal half dynamically contributes more to the overall compaction of PAGE4. Such N- and C-terminal conformational dynamics of PAGE4 and its different phophoforms were also monitored in an early smFRET experiment where the N terminal size variability was measured by probing the distance between residues 18 and 63.25 Interactions between residues 18 and 63 and between residues 63 and 102 were calculated for every conformation in the ELViM projection, and the results show good agreement with experimental observations while validating the well-behaved representation of the data; see Figure 3. Consistent with the present ELViM, our previous observations employing smFRET also indicated that the C-

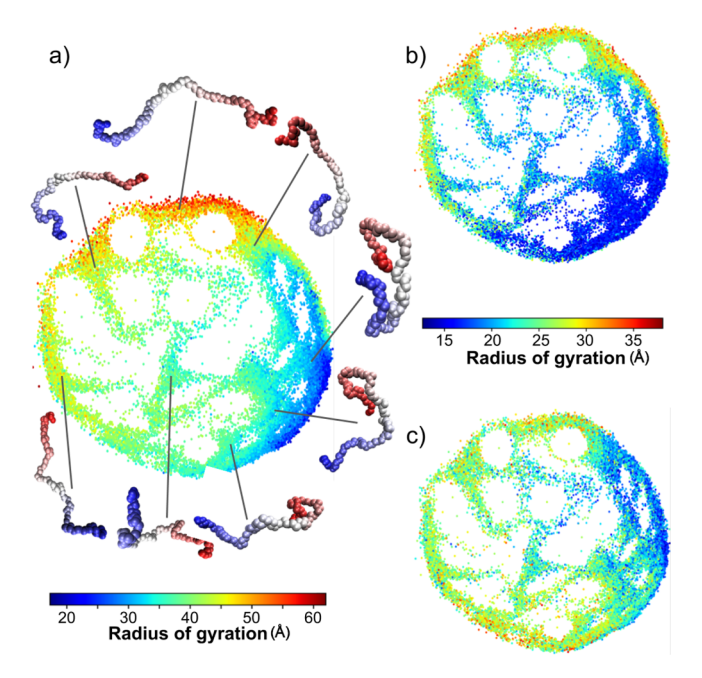


Figure 2. Structures as a function of the radius of gyration. Each conformation is colored as a function of the radius of gyration of (a) the entire protein, (b) the N-terminal part (residues 1–51), and (c) the C-terminal part (residues 52–102); the two small figures have the same colorbar. The shown structures are typical examples of each area of the 2D effective phase space, in which the N- and C-terminals are shown in red and blue, respectively.

terminal region of PAGE4 is less dynamic in terms of its conformational preferences in response to phosphorylation compared to its N-terminal half. As shown in Figure 3, the overall macroscopic size variability of this IDP and its different phosphoforms is well characterized as a function of $R_{\rm g}$. On the other hand, additional work is needed to determine how the segmental loop-forming tendency evolves microscopically in each ensemble.

Analysis of Each PAGE4 Phosphoform. Once all conformations of the data set are projected into the 2D effective phase space, one can start analyzing each ensemble data separately. Because all conformations are described under the same overall reference frame, comparisons between their behavior can be carried out simultaneously. A straightforward analysis is to obtain from the 2D DOS of each pixel i for each PAGE4 conformer (n_i^p) , which is shown in Figure 4. The DOS demonstrates that WT- and HIPK1-PAGE4 populate very distinct areas of conformations compared to CLK2-PAGE4. Also, CLK2-PAGE4 being a more expanded variant, its disorderedness and diminished affinity for c-Jun were very well-characterized in previous biophysical experimental measurements and simulation studies. 25,27,42,43,45 Furthermore, while WT- and HIPK1-PAGE4 can bind to c-Jun, CLK2-PAGE4 has a significantly lower binding affinity for c-Jun. 25,45 Thus, in the current study, we are more interested in analyzing and comparing the conformational heterogeneity between WT- and HIPK1-PAGE4. Interestingly, all previous measurements employing smFRET, NMR, and SAXS showed that HIPK1-PAGE4 is slightly more compact than WT-PAGE4²⁵ Subsequently, experimental measurements also found that in comparison to WT, HIPK1-PAGE4 has reduced binding affinity for c-Jun, which affects its transactivation of target genes. 45 Therefore, to understand the differences between

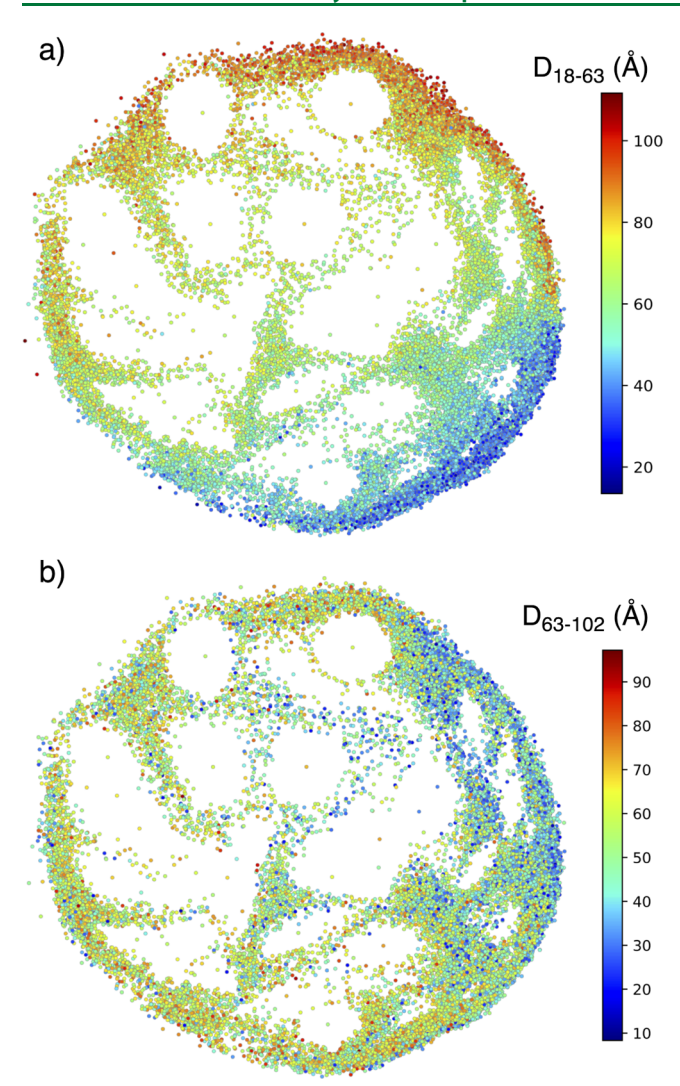


Figure 3. Distances measured by smFRET probes²⁵ are calculated for each conformation in the ELViM projection and colored accordingly. The distances are (a) between residues 18 and 63 and (b) between residues 63 and 102.

WT- and HIPK1-PAGE4, we compared their DOS maps where the effective phase space appears very similar, and in both the maps, we identify three distinct conformational clusters designated as: A, B, and C in Figure 4a,b.

A detailed analysis of these regions can provide insight into the overall features of these states and help in explaining the microscopic origin of the increased compaction in HIPK1-PAGE4 than that seen in WT-PAGE4 as determined by SAXS measurements.²⁵ Region A is the highly populated stable region for WT- and HIPK1-PAGE4 in the entire phase space. It isolates the most compact conformations where the compaction of both the N-terminal 1-51 and C-terminal (52-102) results in lowering of the overall (R_{σ}) value as shown in Figure 2. Regions B and C also have a compact N-terminal region but they possess a more labile and extended C-terminal fraction. The contact maps associated with these regions corroborate this compactness feature. For a given conformation, a contact between residues i and j is considered formed if $r_{ii} \le r_{ci}$, where r_{ci} is the cutoff contact distance. In this study, $r_{ci} = r_{ci}$ 8 Å. For a given set of structures, a contact is considered as formed if it occurs in at least 50% of the states. Figure 5 shows the contact map of WT-PAGE4 and HIPK1-PAGE4 in regions A, B, and C defined in Figure 4a,b. They show contacts between residues involved in the N-terminal portion, characteristic of loop formation. As the system goes from region A to B and C, one can identify a progressive C-terminal region extension. Typical structures of these regions are shown in Figures 2 and 6a-c.

Fly-Casting of Wild-Type PAGE4. Our contact map analysis correlates well with earlier NMR spectroscopy results, which show that PAGE4 has local and long-range conformational preferences that are significantly perturbed by the sitespecific phosphorylation at Thr51.27 It is evident that in WT PAGE4, these preferential interactions are clearly manifested in the N-terminal loop formation, keeping C-terminal relatively extended and exposing the central acidic region where c-Jun binds.²⁷ Our results suggest that such favorable WT-PAGE4 conformations facilitating c-Jun docking to occur are associated with states observed in region C in Figure 4a. The high stability of region A and the structural similarity between the conformations of A and C regions, together with intermediates from the B region, offer a persuasive argument for a functional mechanism. As we move beyond the stable basin of region A, the C-terminal segment progressively becomes extended. It populates region B, finally reaching region C, which allows better exposure of the central acidic region and its close interaction with the c-Jun complex, as depicted in Figure 6. This population-shift toward region C is likely to ensure PAGE4 functioning by extending its higher capture radius, exposing the binding site to c-Jun but still retaining its

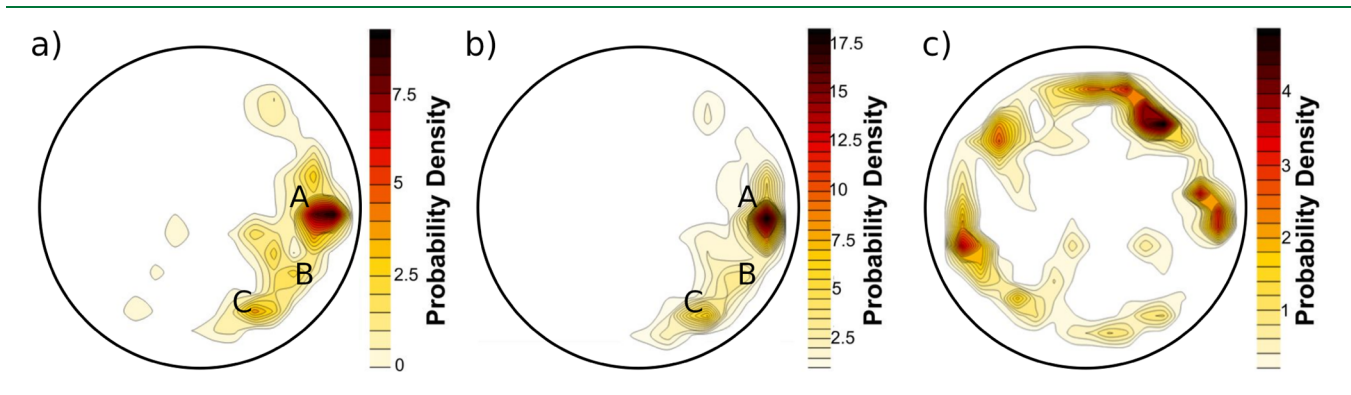


Figure 4. DOS for each phosphoform. Each PAGE4 data set can be analyzed individually using the same 2D effective phase space shown in Figure 1b, from which the DOS is calculated. (a) WT-PAGE4, (b) HIPK1-PAGE4, and (c) CLK2-PAGE4.

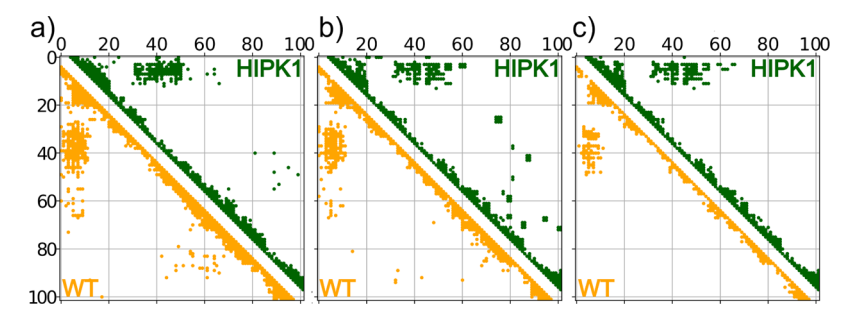


Figure 5. Contact maps for WT-PAGE4 and HIPK1-PAGE4. A residues i and j are defined in contact if they are within a distance r_c ($r_{ij} \le r_{ci}$ with $r_c = 8$. Å). WT-PAGE4 and HIPK1-PAGE4 structures were selected from regions, A, B, and C shown in Figure 4. A contact between residues i and j is considered formed if it occurs in at least 50% of the selected states. The contact maps for regions A, B, and C, are shown in (a-c), respectively. In (c), there are no loop-forming contacts in region C-terminal segments, which indicates that this segment is in its extended form.

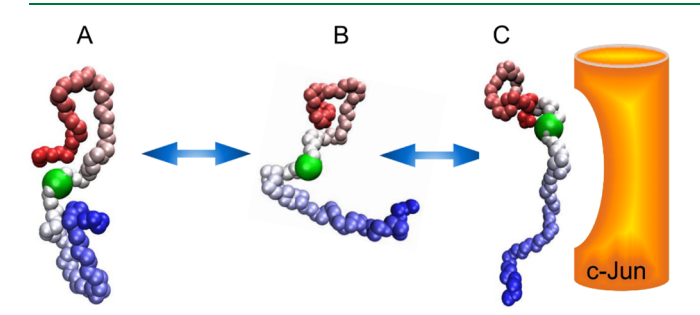


Figure 6. Wild-type PAGE4 mechanism. Suggested fly-casting mechanism of WT-PAGE4, in which the C-terminal portion undergoes a conformational extension, from state A to B and C, allowing it to dock and activate the c-Jun complex. The green highlighted residue corresponds to Thr-51.

moderate flexibility by a partial loop formation. The observation of partial loop formation hints at a fly-casting motion that is frequently observed in the conformational dynamics of disordered proteins. ^{67,68}

Occlusion of HIPK1-PAGE4. Since the 2D conformational phase space of WT- and HIPK1-PAGE4 is very similar, it would be expected that they would have the same binding mechanism to c-Jun. However, experimental results indicate that HIPK1-PAGE4 has a lower binding affinity for c-Jun.² One possible reason for the lowered affinity of HIPK1-PAGE4 for c-Jun in vitro may be due to the more compact nature of the conformational ensemble of HIPK1 than WT-PAGE4. Here, ELViM plays a very important role by capturing the population shift toward region A where both N- and C-terminal regions contribute to form a compact core sequestering the central acidic regions. Such a population shift in HIPK1-PAGE4 renders an occlusion effect barring HIPK1-PAGE4 from interacting with c-Jun, which may reduce their binding affinity as found in experiments.⁴⁵ To qualitatively monitor this population shift mechanism, one can estimate the free energy using eq 3 and the DOS shown in Figure 4. Probing the local minima and saddle points along the path that connects the basins A, B, and C, the approximate free-energy differences can be inferred as $\Delta \mathcal{F}_{i,j} = \mathcal{F}_i - \mathcal{F}_j = k_{\rm B} T \, \log(n_j/n_i)$. The approximate free-energy profiles for WT-PAGE4 and HIPK1-PAGE4 are shown in Figure 7. HIPK1-PAGE4 presents higher energy barriers and higher free-energy difference between basins A and C when compared with WT-PAGE4. Based on both kinetic and thermodynamic aspects, it makes functional conformations in region C less likely to be probed in HIPK1-PAGE4. The energy differences are in the order of

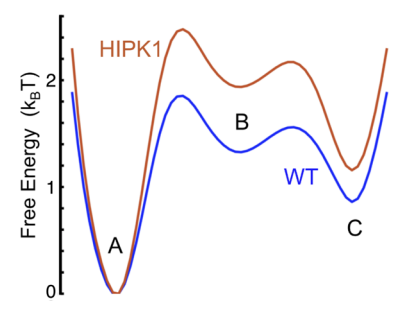


Figure 7. WT- and HIPK1-PAGE4 free energies. Comparison of the free-energy profiles based on the DOS along the path from regions A to B and C. HIPK1-PAGE4 profile presents a higher free-energy difference between A and C ensembles and a higher transition from A to C when compared with WT-PAGE4.

 $k_{\rm B}T$ or less, and hence, it may be argued that these are too small to make a difference in the mechanisms. However, it should be noted that the simulation model is CG, so the values for the energy barriers and free energy difference are qualitative.

Central Role of Thr-51 in Maneuvering Conformational Equilibrium. Biological macromolecules, including IDPs, adopt a diverse ensemble of conformations for which distinct functions have evolved. The populations of conformational ensembles preserve a dynamic equilibrium as we currently find among A, B, and C population regimes. It is clear from our structural analysis that the underlying differences between WT- and HIPK1-PAGE4 have emerged because of the flexibility of the C-terminal motif. The conformational flexibility of the C-terminal motif again depends on its preferential interaction with the acidic region centered on Thr-51. Thus, Thr-51 serves as a controlling anchor, which has the potential to assemble both N- and Cterminals making 8-ring like structures (region A). In HIPK1-PAGE4, the population shift occurs from region C to A which is highly enriched by such 8-ring like structures where Thr-51 is highly buried by the neighboring residues. This feature is readily inferred by measuring the radius of gyration (R_{o}) of segments around Thr-51. We calculate $R_{\rm g}$ in segments from 51 -N to 51 + N for all conformations in the ELViM 2D representation. Figure 8 shows R_g in the intervals [41, 61], [31, 71], [26, 76], and [16, 86] (N = 10, 20, 25, and 35), respectively. The data indicates that the region in which HIPK1-PAGE4 has the highest DOS (region A) corresponds to the lowest R_g , that is, the segment containing Thr-51 in its center is expected to be strongly packed, which is in good

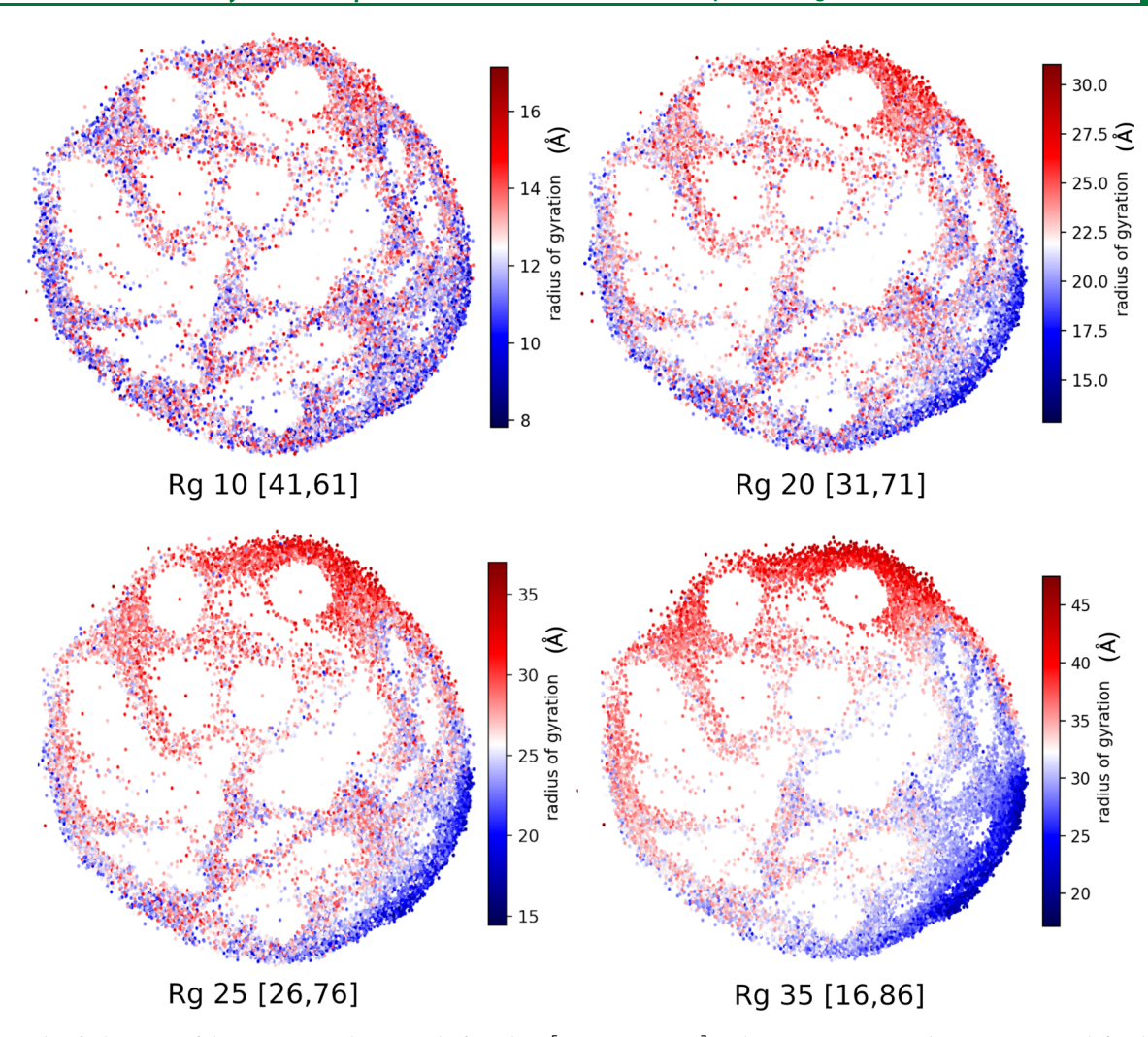


Figure 8. Role of Thr51. R_g of the segment in the interval of residues [51 - N, 51 + N] with N = 10, 20, 25, and 35. In region A defined in Figure 4a,b, R_g is the lowest, which suggests that Thr51 is buried the most, in agreement with experimental results. ²⁵

agreement with the experimental results. This result is also consistent with recent NMR spectroscopic measurements. These measurements revealed that the largest chemical shift occurs at Thr-51, suggesting that Thr-51 envelopes a number of long-range neighbors in the central region. Thus, it becomes more compact and more negatively charged in the HIPK1-PAGE4 version.

CONCLUSIONS

Energy landscapes of IDPs are typically hard to investigate due to the lack of a single native reference conformation. Moreover, due to their plasticity, IDPs tend to explore an unusually larger conformational phase space when compared with classical minimally frustrated proteins, and hence, putative reaction coordinates are practically nonexistent. Even when a posteriori reaction coordinates are found, they have the potential to mask the richness of the dynamics. In contrast, ELViM represents complex multidimensional landscapes in a simplified 2D phase space using a purely data-driven approach, in which no assumption of reaction coordinates or a reference conformation is needed. This reaction-free approach is particularly useful in the case of IDPs. The technique also allows comparisons between proteins studied under different conditions in a single framework.

In the present manuscript, the method was applied to a highly intrinsically disordered protein, PAGE4. The ELViM representation of the data is in excellent agreement with the experimental results obtained using a variety of biophysical techniques. More specifically, the previous computational results, such as the likelihood of loop formation due to phosphorylation and the structural characteristics of the different PAGE4 conformational ensembles, highlight the virtues of employing ELViM to gain deeper insight. In particular, new details of the mechanisms involved in PAGE4 variants are unveiled applying ELViM. For example, hitherto, the WT fly-casting mechanism was thought to be a plausible binding mechanism; 43 however, the ELViM results suggest this may not be the case with HIPK1-PAGE4. The burial of Thr-51, which plays a key role in c-Jun binding, has also been elucidated by analyzing R_{α} in the dominant structural basin of WT- and HIPK1-PAGE4. Considering the ELViM to investigate PAGE4 as a paradigm, it is expected to work equally well for other IDPs and may represent an invaluable tool to address such challenging systems.

AUTHOR INFORMATION

Corresponding Authors

Susmita Roy – Department of Chemical Sciences, Indian Institute of Science Education and Research Kolkata, Mohanpur, West Bengal 741246, India; oorcid.org/0000-0001-6411-4347; Email: susmita.roy@iiserkol.ac.in

Vitor B. P. Leite — Departamento de Física, Instituto de Biociências, Letras e Ciências Exatas, Universidade Estadual Paulista (UNESP), São José do Rio Preto, São Paulo 15054-000, Brazil; ⊚ orcid.org/0000-0003-0008-9079; Email: vitor.leite@unesp.br

Authors

Antonio B. Oliveira Junior — Center for Theoretical Biological Physics, Rice University, Houston, Texas 77005-1892, United States

Xingcheng Lin — Department of Chemistry, Massachusetts Institute of Technology, Cambridge, Massachusetts 02139-4307, United States; ⊙ orcid.org/0000-0002-9378-6174

Prakash Kulkarni – Department of Medical Oncology and Therapeutics Research, City of Hope National Medical Center, Duarte, California 91010, United States

José N. Onuchic — Center for Theoretical Biological Physics, Rice University, Houston, Texas 77005-1892, United States; orcid.org/0000-0002-9448-0388

Complete contact information is available at: https://pubs.acs.org/10.1021/acs.jctc.1c00027

Notes

The authors declare no competing financial interest.

ACKNOWLEDGMENTS

This research was supported by the Center for Theoretical Biological Physics sponsored by the NSF (grants PHY-2019745 and CHE-1614101) and by the Welch Foundation (grant C-1792). A.B.O.J. was funded by FAPESP (São Paulo Research Foundation and Higher Education Personnel) grant 2016/01343-7 and is currently a Robert A. Welch Postdoctoral Fellow. J.N.O. is a Cancer Prevention and Research Institute of Texas (CPRIT) scholar in Cancer Research. V.B.P.L. was funded by FAPESP grant 2019/22540-3 and 2018/18668-1 and Conselho Nacional de Desenvolvimento Científico e Tecnológico (CNPq). S.R. acknowledges support from the Science and Engineering Research Board (grant SRG/2020/001295) and the Department of Biotechnology, Govt. of India (grant BT/12/IYBA/2019/12).

■ REFERENCES

- (1) Anfinsen, C. B. Principles that govern the folding of protein chains. *Science* **1973**, *181*, 223–230.
- (2) Dyson, H. J.; Wright, P. E. Intrinsically unstructured proteins and their functions. *Nat. Rev. Mol. Cell Biol.* **2005**, *6*, 197–208.
- (3) Oldfield, C. J.; Dunker, A. K. Intrinsically Disordered Proteins and Intrinsically Disordered Protein Regions. *Annu. Rev. Biochem.* **2014**, *83*, 553–584.
- (4) Peng, Z.; Yan, J.; Fan, X.; Mizianty, M. J.; Xue, B.; Wang, K.; Hu, G.; Uversky, V. N.; Kurgan, L. Exceptionally abundant exceptions: comprehensive characterization of intrinsic disorder in all domains of life. *Cell. Mol. Life Sci.* **2015**, *72*, 137–151.
- (5) Kulkarni, P.; Uversky, V. N. Intrinsically Disordered Proteins: The Dark Horse of the Dark Proteome. *Proteomics* **2018**, *18*, 1800061.
- (6) Uversky, V. N. Functional roles of transiently and intrinsically disordered regions within proteins. FEBS J. 2015, 282, 1182–1189.
- (7) Wright, P. E.; Dyson, H. J. Intrinsically disordered proteins in cellular signalling and regulation. *Nat. Rev. Mol. Cell Biol.* **2015**, *16*, 18–29.

- (8) Uversky, V. N. Dancing protein clouds: Intrinsically disordered proteins in health and disease, Part A. In *Progress in Molecular Biology and Translational Science*; Uversky, V. N., Ed.; Academic Press, 2019; Vol. 166, pp 1–17.
- (9) Dosztányi, Z.; Chen, J.; Dunker, A. K.; Simon, I.; Tompa, P. Disorder and sequence repeats in hub proteins and their implications for network evolution. *J. Proteome Res.* **2006**, *5*, 2985–2995.
- (10) Tompa, P. Unstructural biology coming of age. Curr. Opin. Struct. Biol. 2011, 21, 419-425.
- (11) Uversky, V. N. Paradoxes and wonders of intrinsic disorder: Stability of instability. *Intrinsically Disord. Proteins* **2017**, 5, No. e1327757.
- (12) Wright, P. E.; Dyson, H. J. Intrinsically unstructured proteins: re-assessing the protein structure-function paradigm. *J. Mol. Biol.* **1999**, 293, 321–331.
- (13) Uversky, V. N.; Dunker, A. K. Understanding protein non-folding. *Biochim. Biophys. Acta Protein Proteonomics* **2010**, 1804, 1231–1264.
- (14) Thirumalai, D.; O'Brien, E. P.; Morrison, G.; Hyeon, C. Theoretical Perspectives on Protein Folding. *Annu. Rev. Biophys.* **2010**, *39*, 159–183.
- (15) Onuchic, J. N.; Wolynes, P. G. Theory of protein folding. *Curr. Opin. Struct. Biol.* **2004**, *14*, 70–75.
- (16) Hills, R.; Brooks, C. Insights from Coarse-Grained Go Models for Protein Folding and Dynamics. *Int. J. Mol. Sci.* **2009**, *10*, 889–905.
- (17) Chebaro, Y.; Ballard, A. J.; Chakraborty, D.; Wales, D. J. Intrinsically Disordered Energy Landscapes. Sci. Rep. 2015, 5, 10386.
- (18) Chong, S.-H.; Ham, S. Folding Free Energy Landscape of Ordered and Intrinsically Disordered Proteins. *Sci. Rep.* **2019**, *9*, 14927.
- (19) Jensen, M. R.; Zweckstetter, M.; Huang, J.-r.; Blackledge, M. Exploring Free-Energy Landscapes of Intrinsically Disordered Proteins at Atomic Resolution Using NMR Spectroscopy. *Chem. Rev.* **2014**, *114*, 6632–6660.
- (20) Chen, T.; Song, J.; Chan, H. S. Theoretical perspectives on nonnative interactions and intrinsic disorder in protein folding and binding. *Curr. Opin. Struct. Biol.* **2015**, *30*, 32–42.
- (21) İakoucheva, L. M.; Radivojac, P.; Brown, C. J.; O'Connor, T. R.; Sikes, J. G.; Obradovic, Z.; Dunker, A. K. The importance of intrinsic disorder for protein phosphorylation. *Nucleic Acids Res.* **2004**, 32, 1037–1049.
- (22) Niklas, K. J.; Dunker, A. K.; Yruela, I. The evolutionary origins of cell type diversification and the role of intrinsically disordered proteins. *J. Exp. Bot.* **2018**, *69*, 1437–1446.
- (23) Hendus-Altenburger, R.; Lambrughi, M.; Terkelsen, T.; Pedersen, S. F.; Papaleo, E.; Lindorff-Larsen, K.; Kragelund, B. B. A phosphorylation-motif for tuneable helix stabilisation in intrinsically disordered proteins Lessons from the sodium proton exchanger 1 (NHE1). *Cell. Signal.* **2017**, *37*, 40–51.
- (24) Bah, A.; Forman-Kay, J. D. Modulation of Intrinsically Disordered Protein Function by Post-translational Modifications. *J. Biol. Chem.* **2016**, 291, 6696–6705.
- (25) Kulkarni, P.; Jolly, M. K.; Jia, D.; Mooney, S. M.; Bhargava, A.; Kagohara, L. T.; Chen, Y.; Hao, P.; He, Y.; Veltri, R. W.; Grishaev, A.; Weninger, K.; Levine, H.; Orban, J. Phosphorylation-induced conformational dynamics in an intrinsically disordered protein and potential role in phenotypic heterogeneity. *Proc. Natl. Acad. Sci.* **2017**, *114*. E2644—E2653.
- (26) Sicoli, G.; Kress, T.; Vezin, H.; Ledolter, K.; Kurzbach, D. A Switch between Two Intrinsically Disordered Conformational Ensembles Modulates the Active Site of a Basic-Helix-Loop-Helix Transcription Factor. J. Phys. Chem. Lett. 2020, 11, 8944–8951.
- (27) He, Y.; Chen, Y.; Mooney, S. M.; Rajagopalan, K.; Bhargava, A.; Sacho, E.; Weninger, K.; Bryan, P. N.; Kulkarni, P.; Orban, J. Phosphorylation-induced Conformational Ensemble Switching in an Intrinsically Disordered Cancer/Testis Antigen. *J. Biol. Chem.* **2015**, 290, 25090–25102.

- (28) Ulmer, T. S.; Bax, A.; Cole, N. B.; Nussbaum, R. L. Structure and dynamics of micelle-bound human alpha-synuclein. *J. Biol. Chem.* **2005**, 280, 9595–9603.
- (29) Wells, M.; Tidow, H.; Rutherford, T. J.; Markwick, P.; Jensen, M. R.; Mylonas, E.; Svergun, D. I.; Blackledge, M.; Fersht, A. R. Structure of tumor suppressor p53 and its intrinsically disordered N-terminal transactivation domain. *Proc. Natl. Acad. Sci. U.S.A.* 2008, 105, 5762–5767.
- (30) Sibille, N.; Bernadó, P. Structural characterization of intrinsically disordered proteins by the combined use of NMR and SAXS. *Biochem. Soc. Trans.* **2012**, *40*, 955–962.
- (31) Nasir, I.; Onuchic, P. L.; Labra, S. R.; Deniz, A. A. Single-molecule fluorescence studies of intrinsically disordered proteins and liquid phase separation. *Biochim. Biophys. Acta Protein Proteonomics* **2019**, *1867*, 980–987.
- (32) Das, R. K.; Pappu, R. V. Conformations of intrinsically disordered proteins are influenced by linear sequence distributions of oppositely charged residues. *Proc. Natl. Acad. Sci. U.S.A.* **2013**, *110*, 13392–13397.
- (33) Fuertes, G.; et al. Decoupling of size and shape fluctuations in heteropolymeric sequences reconciles discrepancies in SAXS vs. FRET measurements. *Proc. Natl. Acad. Sci. U.S.A.* **2017**, *114*, E6342–E6351.
- (34) Emperador, A.; Sfriso, P.; Villarreal, M. A.; Gelpí, J. L.; Orozco, M. PACSAB: Coarse-Grained Force Field for the Study of Protein—Protein Interactions and Conformational Sampling in Multiprotein Systems. *J. Chem. Theory Comput.* **2015**, *11*, 5929—5938.
- (35) Knott, M.; Best, R. B. Discriminating binding mechanisms of an intrinsically disordered protein via a multi-state coarse-grained model. *J. Chem. Phys.* **2014**, *140*, 175102.
- (36) Wu, H.; Wolynes, P. G.; Papoian, G. A. AWSEM-IDP: A Coarse-Grained Force Field for Intrinsically Disordered Proteins. *J. Phys. Chem. B* **2018**, *122*, 11115–11125.
- (37) Marsh, J. A.; Forman-Kay, J. D. Ensemble modeling of protein disordered states: experimental restraint contributions and validation. *Proteins* **2012**, *80*, 556–572.
- (38) Schneider, R.; Huang, J.-r.; Yao, M.; Communie, G.; Ozenne, V.; Mollica, L.; Salmon, L.; Jensen, M. R.; Blackledge, M. Towards a robust description of intrinsic protein disorder using nuclear magnetic resonance spectroscopy. *Mol. Biosyst.* **2012**, *8*, 58–68.
- (39) Best, R. B.; Zheng, W.; Mittal, J. Balanced Protein–Water Interactions Improve Properties of Disordered Proteins and Non-Specific Protein Association. *J. Chem. Theory Comput.* **2014**, *10*, 5113–5124.
- (40) Ferrie, J. J.; Petersson, E. J. A Unified De Novo Approach for Predicting the Structures of Ordered and Disordered Proteins. *J. Phys. Chem. B* **2020**, *124*, 5538–5548.
- (41) Henriques, J.; Cragnell, C.; Skepö, M. Molecular Dynamics Simulations of Intrinsically Disordered Proteins: Force Field Evaluation and Comparison with Experiment. *J. Chem. Theory Comput.* **2015**, *11*, 3420–3431.
- (42) Lin, X.; Roy, S.; Jolly, M. K.; Bocci, F.; Schafer, N. P.; Tsai, M.-Y.; Chen, Y.; He, Y.; Grishaev, A.; Weninger, K.; Orban, J.; Kulkarni, P.; Rangarajan, G.; Levine, H.; Onuchic, J. N. PAGE4 and Conformational Switching: Insights from Molecular Dynamics Simulations and Implications for Prostate Cancer. *J. Mol. Biol.* **2018**, 430, 2422–2438.
- (43) Lin, X.; et al. Structural and Dynamical Order of a Disordered Protein: Molecular Insights into Conformational Switching of PAGE4 at the Systems Level. *Biomolecules* **2019**, *9*, 77.
- (44) Rajagopalan, K.; Qiu, R.; Mooney, S. M.; Rao, S.; Shiraishi, T.; Sacho, E.; Huang, H.; Shapiro, E.; Weninger, K. R.; Kulkarni, P. The Stress-response protein prostate-associated gene 4, interacts with c-Jun and potentiates its transactivation. *Biochim. Biophys. Acta (BBA)-Mol. Basis Dis.* **2014**, *1842*, 154–163.
- (45) Mooney, S. M.; Qiu, R.; Kim, J. J.; Sacho, E. J.; Rajagopalan, K.; Johng, D.; Shiraishi, T.; Kulkarni, P.; Weninger, K. R. Cancer/testis antigen PAGE4, a regulator of c-Jun transactivation, is phosphorylated

- by homeodomain-interacting protein kinase 1, a component of the stress-response pathway. *Biochemistry* **2014**, *53*, 1670–1679.
- (46) Zeng, Y.; He, Y.; Yang, F.; Mooney, S. M.; Getzenberg, R. H.; Orban, J.; Kulkarni, P. The cancer/testis antigen prostate-associated gene 4 (PAGE4) is a highly intrinsically disordered protein. *J. Biol. Chem.* 2011, 286, 13985–13994.
- (47) Oliveira, A. B.; Yang, H.; Whitford, P. C.; Leite, V. B. P. Distinguishing Biomolecular Pathways and Metastable States. *J. Chem. Theory Comput.* **2019**, *15*, 6482–6490.
- (48) Chen, M.; Lin, X.; Zheng, W.; Onuchic, J. N.; Wolynes, P. G. Protein Folding and Structure Prediction from the Ground Up: The Atomistic Associative Memory, Water Mediated, Structure and Energy Model. *J. Phys. Chem. B* **2016**, *120*, 8557–8565.
- (49) Chen, M.; Lin, X.; Lu, W.; Onuchic, J. N.; Wolynes, P. G. Protein Folding and Structure Prediction from the Ground Up II: AAWSEM for α/β Proteins. *J. Phys. Chem. B* **2017**, *121*, 3473–3482.
- (50) Davtyan, A.; Schafer, N. P.; Zheng, W.; Clementi, C.; Wolynes, P. G.; Papoian, G. A. AWSEM-MD: Protein Structure Prediction Using Coarse-Grained Physical Potentials and Bioinformatically Based Local Structure Biasing. *J. Phys. Chem. B* **2012**, *116*, 8494–8503
- (51) Plimpton, S. Fast Parallel Algorithms for Short-Range Molecular Dynamics. *J. Comput. Phys.* **1995**, *117*, 1–19.
- (52) Huang, J.; Rauscher, S.; Nawrocki, G.; Ran, T.; Feig, M.; de Groot, B. L.; Grubmüller, H.; MacKerell, A. D. CHARMM36m: an improved force field for folded and intrinsically disordered proteins. *Nat. Methods* **2017**, *14*, 71–73.
- (53) Zang, T.; Yu, L.; Zhang, C.; Ma, J. Parallel continuous simulated tempering and its applications in large-scale molecular simulations. *J. Chem. Phys.* **2014**, *141*, 044113.
- (54) Pronk, S.; Páll, S.; Schulz, R.; Larsson, P.; Bjelkmar, P.; Apostolov, R.; Shirts, M.; Smith, J.; M Kasson, P.; van der Spoel, D.; Hess, B.; Lindahl, E. GROMACS 4.5: A high-throughput and highly parallel open source molecular simulation toolkit. *Bioinformatics* **2013**, 29, 845.
- (55) Abraham, M. J.; Murtola, T.; Schulz, R.; Páll, S.; Smith, J. C.; Hess, B.; Lindahl, E. GROMACS: High performance molecular simulations through multi-level parallelism from laptops to supercomputers. *SoftwareX* **2015**, *1-2*, 19–25.
- (56) Schneider, T.; Stoll, E. Molecular-dynamics study of a three-dimensional one-component model for distortive phase transitions. *Phys. Rev. B: Solid State* **1978**, *17*, 1302–1322.
- (57) Tsai, M.-Y.; Zheng, W.; Balamurugan, D.; Schafer, N. P.; Kim, B. L.; Cheung, M. S.; Wolynes, P. G. Electrostatics, structure prediction, and the energy landscapes for protein folding and binding. *Protein Sci.* **2016**, 25, 255–269.
- (58) Shen, T.; Zong, C.; Hamelberg, D.; Andrew Mccammon, J.; Wolynes, P. G. The folding energy landscape and phosphorylation: modeling the conformational switch of the NFAT regulatory domain. *Faseb. J.* **2005**, *19*, 1389–1395.
- (59) Lätzer, J.; Shen, T.; Wolynes, P. G. Conformational Switching upon Phosphorylation: A Predictive Framework Based on Energy Landscape Principles. *Biochemistry* **2008**, *47*, 2110–2122.
- (60) Oliveira, A. B., Jr.; Fatore, F. M.; Paulovich, F. V.; Oliveira, O. N., Jr.; Leite, V. B. P. Visualization of Protein Folding Funnels in Lattice Models. *PloS One* **2014**, *9*, No. e100861.
- (61) Hardin, C.; Eastwood, M. P.; Prentiss, M. C.; Luthey-Schulten, Z.; Wolynes, P. G. Associative memory Hamiltonians for structure prediction without homology: alpha/beta proteins. *PNAS* **2003**, *100*, 1679–1684.
- (62) Ragonnet-Cronin, M.; Hodcroft, E.; Hué, S.; Fearnhill, E.; Delpech, V.; Leigh Brown, A.; Lycett, S. UK HIV Drug Resistance Database, Automated analysis of phylogenetic clusters. *BMC Bioinf.* **2013**, *14*, 317.
- (63) Hinchliff, C. E.; et al. Synthesis of phylogeny and taxonomy into a comprehensive tree of life. *Proc. Natl. Acad. Sci.* **2015**, *112*, 12764–12769.
- (64) Fitch, W. M.; Margoliash, E. Construction of Phylogenetic Trees. *Science* **1967**, *155*, 279–284.

- (65) Felsenstein, J. PHYLIP (PHYLogeny Inference Package), 1980. https://evolution.genetics.washington.edu/phylip.html.
- (66) Lätzer, J.; Papoian, G. A.; Prentiss, M. C.; Komives, E. A.; Wolynes, P. G. Induced Fit, Folding, and Recognition of the NF- κ B-Nuclear Localization Signals by $I\kappa$ B α and $I\kappa$ B β . J. Mol. Biol. 2007, 367, 262–274.
- (67) Levy, Y.; Onuchic, J. N.; Wolynes, P. G. Fly-Casting in Protein-DNA Binding: Frustration between Protein Folding and Electrostatics Facilitates Target Recognition. *J. Am. Chem. Soc.* **2007**, *129*, 738–739.
- (68) Shoemaker, B. A.; Portman, J. J.; Wolynes, P. G. Speeding molecular recognition by using the folding funnel: The fly-casting mechanism. *Proc. Natl. Acad. Sci.* **2000**, *97*, 8868–8873.